Contents lists available at ScienceDirect

Materials Science in Semiconductor Processing

journal homepage: www.elsevier.com/locate/mssp

Highlights

Anatomy of resistive switching behavior in titanium oxide based RRAM device

Materials Science in Semiconductor Processing xxx (xxxx) xxx

Kuan Yang, Liping Fu, Junhao Chen, Fangcong Wang*, Lixue Tian, Xiaoqiang Song, Zewei Wu, Yingtao Li*

- Effectively decrease forming voltage and operating energy of RRAM.
- Explicitly analyze the switching behavior by stochastic numerical physics model.
- Dynamically visualize evolution of conductive filaments to understand the mechanism.

Contents lists available at ScienceDirect

Materials Science in Semiconductor Processing

journal homepage: www.elsevier.com/locate/mssp

Full length article

Anatomy of resistive switching behavior in titanium oxide based RRAM device

Kuan Yang [a,b,1], Liping Fu [a,1], Junhao Chen [c], Fangcong Wang [a,*], Lixue Tian [a], Xiaoqiang Song [a], Zewei Wu [a], Yingtao Li [a,*]

[a] School of Physical Science and Technology, Lanzhou University, Lanzhou 730000, China
[b] Cuiying Honors College, Lanzhou University, Lanzhou 730000, China
[c] School of Mechanical Engineering, University of Leeds, Leeds LS2 9JT, United Kingdom

ARTICLE INFO

Keywords:
Resistive switching
Numerical physics model
Oxygen vacancy
Metal oxide

ABSTRACT

Resistive random access memory (RRAM) devices based on binary transition metal oxides and the application for nonvolatile memory devices are becoming an area of extensive concern. The physical understanding of resistive switching is crucial for RRAM development. In this paper, both experiments and simulated dynamic formation and rupture processes of oxygen vacancy (V_O) conductive filament (CF) channels in titanium oxide based RRAM devices are presented. Compared with the Al/$TiO_{2.1}$/Al device with higher oxygen content, the Al/$TiO_{1.6}$/Al device shows a lower forming voltage. However, little dependence on oxygen content in TiO_x film is shown for other resistive switching parameters, including high resistance state resistance, low resistance state resistance, set voltage, and reset voltage. A numerical physics model is presented to relate the resistive switching behavior with the evolution CF channels in terms of V_O morphology and $I-V$ characteristics.

1. Introduction

Resistive random access memory (RRAM) device based on the binary transition metal oxide is regarded as prospective choice for next-generation nonvolatile memory applications considering its simple structure, excellent scalability, fast speed, low power consumption, and high density [1–5]. Recently, abundant research has been done on titanium oxide film for RRAM applications due to its simple constitution and feasible compatibility with CMOS technology [6–9]. So far, various models, including power-induced mechanism [7], Schottky-emission-type conduction [8], and conductive filament (CF) channels [9], have been utilized to explain the resistive switching behaviors in TiO_x-based RRAM devices. Among existing models, the idea of the formation and disruption of CFs seems to be one of the most plausible [9,10]. Moreover, the evolution and morphology of CFs are believed to affect the electrical performances of RRAM in terms of the forming and the subsequent resistive switching process [11,12]. Nevertheless, the details of microscopic changes of CFs responsible for the resistive switching are still lacking, partly because the initial generation of CFs by electrical forming process is also poorly understood.

In this letter, in order to generalize the resistive switching behavior of TiO_x-based RRAM, we carry out an experimental analysis and also introduce a numerical physics model for insights into V_O CFs during the forming and the subsequent resistive switching process. The model can accurately capture the forming and $I-V$ characteristics of TiO_x-based RRAM devices with different oxygen content in TiO_x films. Such a comprehensive analysis of the V_O CFs formation and rupture would strongly aid the manufacturing of the TiO_x-based device for optimization purposes.

2. Experiments

The cross-point arrays Al/TiO_x/Al memory devices with device areas of 20 μm ×20 μm were fabricated on SiO_2/Si substrates. 200 nm vertical lines of Al as bottom electrodes were first deposited by electron beam evaporation and patterned through a lift-off process. Subsequently, $TiCl_4$ was used as the Ti precursor and H_2O was used as the oxygen precursor. An atomic layer deposition cycle with four steps was adopted for this experiment. The four steps were $TiCl_4$ reactant, N_2 purge, H_2O reactant, and N_2 purge, respectively. The pulse durations of the $TiCl_4$ and N_2 were 200 ms and 1500 ms, respectively. In order to investigate the effect of oxygen content on the resistive switching characteristics of titanium oxide films, two sets of TiO_x (30 nm) devices with different oxygen content were defined by the pulse durations of the H_2O with 250 ms and 450 ms, respectively. By using X-ray

* Corresponding authors.
E-mail addresses: wangfc@lzu.edu.cn (F. Wang), li_yt06@lzu.edu.cn (Y. Li).
[1] K. Yang and L. Fu contribute equally to this work

https://doi.org/10.1016/j.mssp.2022.106492
Received 15 August 2021; Received in revised form 5 December 2021; Accepted 12 January 2022

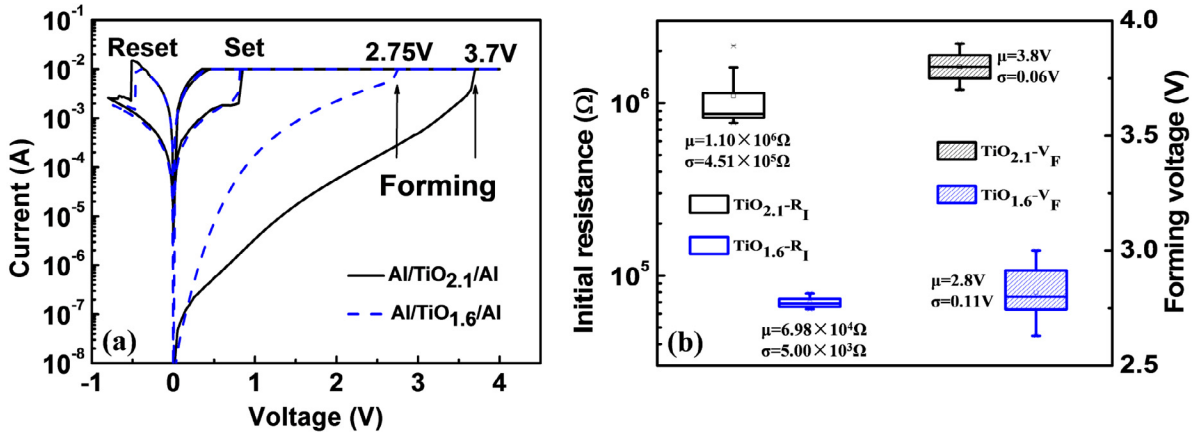

Fig. 1. (a) Typical *I-V* curves of the Al/$TiO_{2.1}$/Al device and Al/$TiO_{1.6}$/Al device. (b) Statistical distributions of the initial resistances (R_I) and forming voltages (V_F) of both devices from 20 randomly chosen fresh devices.

photoelectron spectroscopy (XPS) analyses, the oxygen to titanium ratio of the as prepared films for the two sets of TiO_x devices was about 1.6 and 2.1, respectively. Finally, 200 nm horizontal lines of Al as top electrodes were deposited by electron beam evaporation after the last lithography, and then another lift-off process was used to pattern the top electrodes. A Keithley 4200-SCS semiconductor characterization system was applied for measurement of all electrical characteristics. During the measurements, the top electrode was biased with the bottom electrode grounded.

3. Results and discussion

Fig. 1(a) shows the typical $I-V$ curves of the Al/$TiO_{2.1}$/Al and Al/$TiO_{1.6}$/Al devices. Both devices show high initial resistances, and to trigger the reversible resistive switching behaviors in both devices, an electroforming process through the utilization of a large positive voltage is essential. After the initial electroforming process, both devices can be switched from the low resistance state (LRS) to a high resistance state (HRS) (reset process) by applying a negative bias, and through a positive voltage to switch from the HRS to the LRS (set process) again, as shown in Fig. 1(a). For each structure, a group of 20 fresh devices are selected randomly, and the statistics of the initial resistances (R_I) and forming voltages (V_F) are shown in Fig. 1(b). For each structure, a group of 20 fresh devices are selected randomly, and the statistics of the initial resistances (R_I) and forming voltages (V_F) are shown in Fig. 1(b), in which $TiO_{2.1} - R_I$ and $TiO_{1.6} - R_I$ represent the initial resistances of the Al/$TiO_{2.1}$/Al and Al/$TiO_{1.6}$/Al device, and the $TiO_{2.1} - V_F$ and $TiO_{1.6} - V_F$ represent the forming voltages of the Al/$TiO_{2.1}$/Al and Al/$TiO_{1.6}$/Al device. It should be noted that the mean value (μ) of R_I for the Al/$TiO_{1.6}$/Al device is lower than that of the Al/$TiO_{2.1}$/Al devices, and the μ of V_F is reduced from 3.8 V to 2.8 V for the Al/$TiO_{1.6}$/Al device. The lower V_F is natural for the Al/$TiO_{1.6}$/Al device, as an active layer with lower O/Ti ratio shares relatively higher oxygen vacancy concentration [13], which contributes to the higher leakage current. It has been demonstrated that the forming voltage of RRAM device is partly controlled by the thickness of the oxide films. In other words, the forming voltage would drop as the film thickness decreases [14]. In our case, the large forming voltage is due to the fact that 30 nm TiO_x film was used, and it is conceivable that the forming voltage would decrease if a thinner film thickness is applied [14].

Fig. 2(a) and Fig. 2(b) show the device-to-device distributions of HRS resistance (R_H), LRS resistance (R_L), set voltage (V_S), and reset voltage (V_R) for both devices, all these statistical data are from the repeatability of the resistive switching loops. As shown in Fig. 2, the μ of R_H, R_L, V_S and V_R for the two devices are almost the same, indicating that the resistive switching parameters, including R_H, R_L, V_S, and V_R, show little dependence on oxygen content in as-deposited TiO_x film.

To deeply investigate why these two devices behave so distinctively, a numerical physics model which takes factors temperature, electrical field, current density into consideration is presented based on Monte Carlo simulation to analyze the *I-V* characteristics and the related V_O CFs evolution during the forming and the subsequent resistive switching process. The simulation compromises two modules, including the calculation for generation and recombination of V_O, and the motion of O^{2-}, in addition, the configuration of electrical field and temperature which is essential for simulation is calculated as well. The results from the simulation show a straightforward dynamical process of formation and rupture of CFs.

At first, the filament region is split into grids of 30 × 60. To represent different types of TiO_x material, the computational domain is set to different initial state of V_O concentration and configuration. The generation and recombination of V_O are simulated according to the possibility in (1) and (2), respectively [15].

$$P_G = \upsilon \exp(-\frac{E_A - b \cdot F}{k_B \cdot T}) \tag{1}$$

$$P_R = \upsilon \exp(-\frac{E_{A,R}}{k_B \cdot T}) \tag{2}$$

where $\upsilon = 1.9 \times 10^{13}$ Hz is the effective vibration frequency of the O–Ti bonds [16], $E_A = 2.02$ eV [17] is the zero-field effective activation energy required to break the Ti–O bond, F is the local electrical field, b is the bond polarization factor, taken as 180eV in our simulation, which is in good agreement with reported experimental result [15]. $E_{A,R} = 0.2$ eV is the activation energy, and k_B, T are Boltzmann constant and local temperature, respectively [15].

The motion of oxygen ion at grid i is modeled based on its rate R_D[15], given by:

$$R_D = \upsilon \exp\left(-\frac{E_{A,D} - k_D \cdot F_D}{k_B \cdot T}\right) \tag{3}$$

$E_{A,D}$ is equal to 0.7 eV for oxygen ions, and $k_D = qd_0\lambda$ is a factor accounting for the field-induced energy barrier reduction [18], where $d_0 = 5 \times 10^{-10}$m is the mesh size in simulation, and $\lambda \cdot d_0 = |i - j| \cdot d_0$ denotes the distance to the available grid j from grid i. F_D is the electrical field along the diffusion direction [15].

The local temperature T is solved by the Fourier equation [19], namely

$$\nabla k_{th} \nabla T = \sigma |\nabla V|^2 \tag{4}$$

where k_{th}, σ are thermal conductivity and electrical conductivity, respectively, which are variables to temperature or V_O concentration. The

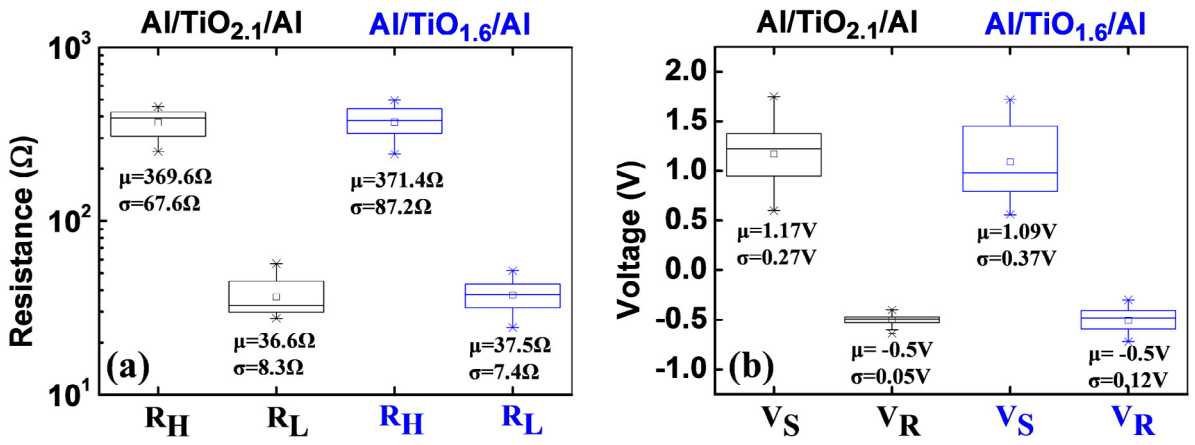

Fig. 2. Statistical distributions of resistive switching parameters for the Al/$TiO_{2.1}$/Al device and Al/$TiO_{1.6}$/Al device. (a) HRS resistance (R_H) and LRS resistances (R_L), (b) set voltage (V_S) and reset voltage (V_R).

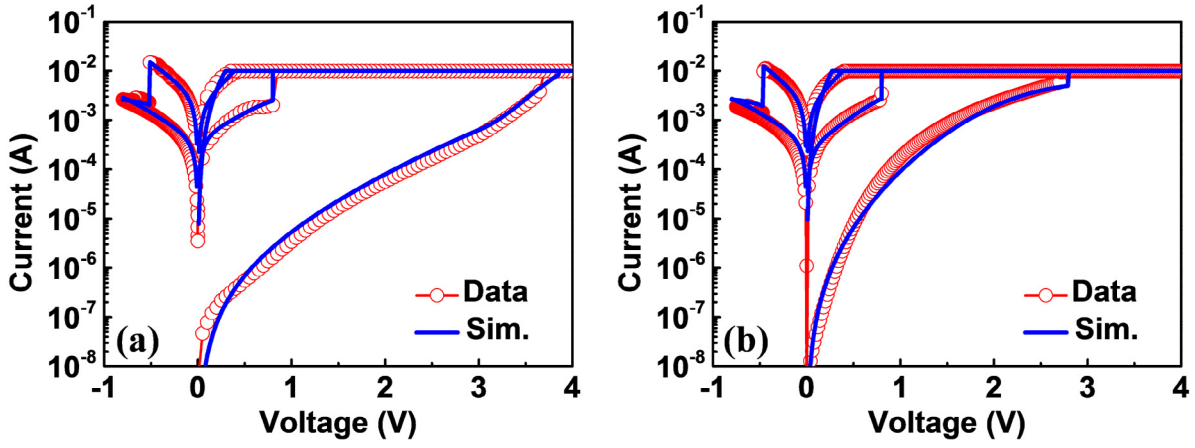

Fig. 3. Comparison between experimental and simulated *I-V* characteristics of (a) Al/$TiO_{2.1}$/Al device and (b) Al/$TiO_{1.6}$/Al device.

electrical conductivity σ is given by [20]

$$\sigma = \sigma_0 \exp\left(-\frac{E_{AC}}{k_B T}\right) \tag{5}$$

where σ_0 is the pre-exponential factor, E_{AC} is the activation energy for electrical conduction [21].

The electrical field F and F_D are solved by Poisson Equation, namely

$$\nabla^2 \phi = -\frac{\rho}{\epsilon_0} \tag{6}$$

with the boundary condition as $\phi = 0$ and $\phi = V_d$, where V_d is the applied bias, ρ is the distribution of charges, and ϵ_0 is the permittivity of the free space.

Moreover, we calculate the current by combining the ionic conduction of the V_O, and the conduction through electrons. Hence, the current can be calculated by the following equation [21],

$$I = I_0 \exp\left(-\frac{a}{a_0}\right) \sinh\left(\frac{V}{V_0}\right) + N q v_d \tag{7}$$

where $I_0 \approx 0.1nA, a \approx 1\ nm, a_0 \approx 0.05\ nm, V_0 \approx 0.4V$ [16] are parameters of the hopping conduction of V_O at the low bias region. N is the number of traps participating in the tunneling process given by

$$N = n_D \cdot n_0 \tag{8}$$

where n_D is the vertical oxygen vacancy participating in tunneling, which is computed by the configuration of V_O, and $n_0 \sim 10^{16}$ is the parameter obtained by curve fitting at LRS region since the n_D we obtained is in 2D cross section, and we have to amplify it to satisfy the conduction in 3D scale, and v_d is the transition rate, given by [21,22]

$$v_d = a_d \cdot v_0 \cdot \exp\left(-\frac{E_a}{k_B T}\right) \cdot \sinh\left(\frac{2qFa_d}{k_B T}\right) \tag{9}$$

where F is the local electrical field solved by (6), $a_d = 0.1nm$ is the effective hopping distance, v_0 is the attempt-to-escape frequency of 10^{13} Hz [21,22].

Finally, we combine all the equations with the framework of the numerical model. After providing the model with the initial condition, we could subsequently calculate the evolution of V_O, and update the temperature and electric field. We would keep iterating the computation till the system approaches the convergence under the given bias. The system would prompt to the next step of bias once it converges.

Fig. 3(a) and Fig. 3(b) show the simulated and the experimental curves of forming process and subsequent resistive switching for the Al/$TiO_{2.1}$/Al device and Al/$TiO_{1.6}$/Al device, respectively. It is noted that the simulated results agree well with experimental data for both devices. The forming process and the consequent resistive switching characteristics are well captured by the analytical model.

Dynamics of V_O migration effect on CFs growth in TiO_x films is analyzed afterwards. To ensure the representativeness of the results, we iterate the simulation for 100 times. Fig. 4 shows the simulated dynamic evolution of V_O CFs during the forming and the subsequent resistive switching process for both Al/$TiO_{2.1}$/Al device (images a–h) and Al/$TiO_{1.6}$/Al device (images i–p). For Al/$TiO_{2.1}$/Al device, the CF grows from the bottom of the device, and it continues to grow as the bias increases. The tip of the CF extends gradually, and it finally reaches the

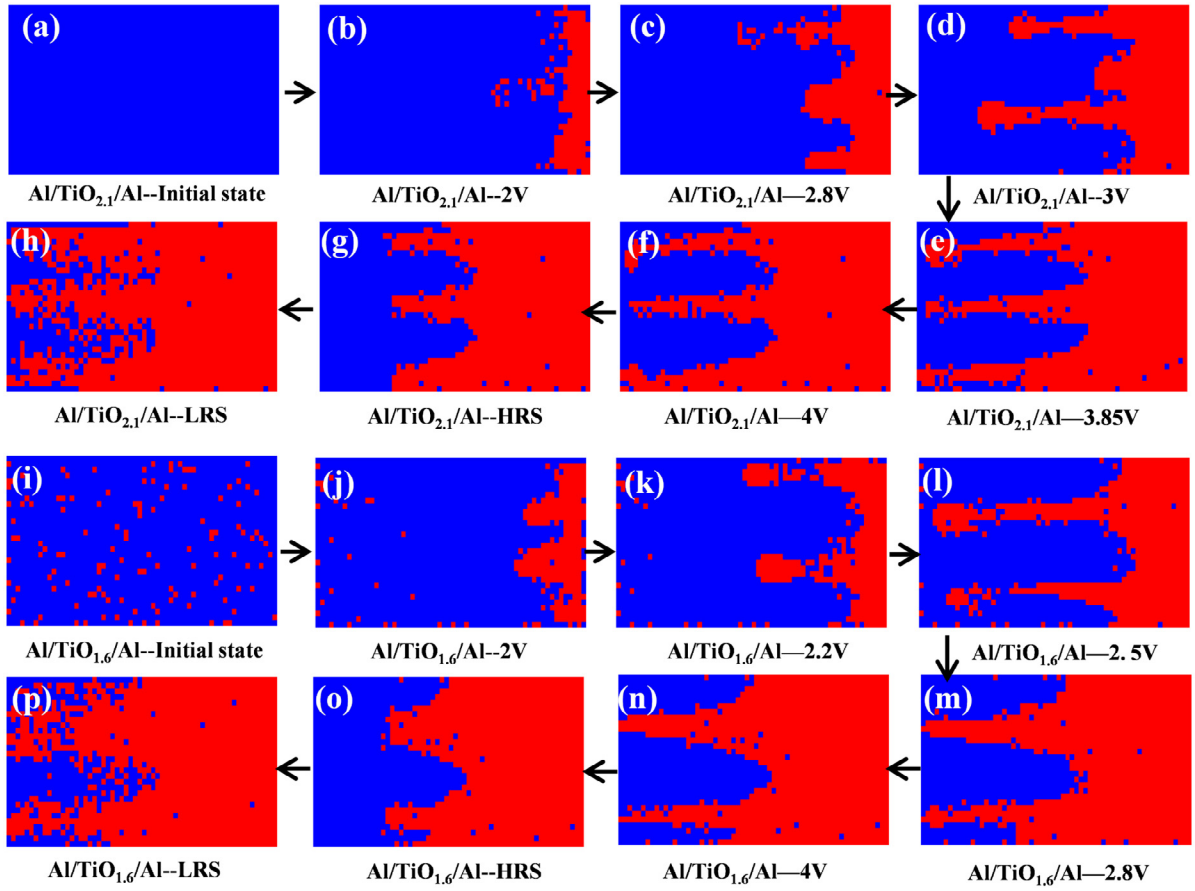

Fig. 4. Simulated dynamic structure evolution of V_O CFs in both Al/$TiO_{2.1}$/Al device (a–h) and Al/$TiO_{1.6}$/Al device (i–p).

top side of the device at 3.85 V. Then, the CF grows thicker when the bias keeps increasing. When resetting the device, the CF breaks at the tip near the top electrode and it resumes when a positive bias is applied in SET process. The case of Al/$TiO_{1.6}$/Al is similar, however, the CF grows faster and is thicker. To be specific, for the Al/$TiO_{2.1}$/Al device, V_O CFs bridge the top electrode and bottom electrode when the voltage reaches 3.85 V. However, for the Al/$TiO_{1.6}$/Al device, V_O CF channels form once the voltage increases to 2.8 V. This happens because more V_Os exist in the $TiO_{1.6}$ film than the $TiO_{2.1}$ film. Therefore, compared with the Al/$TiO_{2.1}$/Al device, a lower voltage is enough to form the V_O CF channels in the Al/$TiO_{1.6}$/Al device. Furthermore, when the voltage increases to 4 V, the morphology of CF channels in the Al/$TiO_{1.6}$/Al device (image n) is quite similar to that in the Al/$TiO_{2.1}$/Al device (image f). Evidently, in the case of the subsequent resistive switching process, the morphology of CF channels of both HRS (image g versus image o) and LRS (image h versus image p) in the two devices is similar. Thus, the R_H and R_L of the two devices are almost the same, as shown in Fig. 2(a).

4. Conclusion

In summary, an experimental analysis was performed to investigate the effect of oxygen content in titanium oxide films on the performance of Al/TiO_x/Al RRAM devices. In addition, a numerical physics model was presented to describe the detailed evolution of the formation and rupture of V_O CFs during the forming and the subsequent resistive switching process. The simulated *I-V* characteristics are in good agreement with the experimental data, which enhances the understanding towards the underlying mechanism of resistive switching and can further optimize the performance of a metal oxide-based RRAM device.

CRediT authorship contribution statement

Kuan Yang: Conceptualization, Methodology, Software, Investigation, Writing – original draft. **Liping Fu:** Investigation, Data curation, Writing – original draft. **Junhao Chen:** Conceptualization, Formal Analysis, Writing – review & editing. **Fangcong Wang:** Supervision. **Lixue Tian:** Resources. **Xiaoqiang Song:** Resources. **Zewei Wu:** Resources. **Yingtao Li:** Conceptualization, Investigation, Data curation, Supervision, Writing – review & editing, Funding acquisition.

Acknowledgments

This work was supported by the National Natural Science Foundation of China (Grant No. 61774079), the Science and Technology Plan of Gansu Province (No. 20JR5RA307), the Key Talent Project of Organization Department in Gansu Province, the Hui-Chun Chin and Tsung-Dao Lee Chinese Undergraduate Research Endowment (LZU - JZH2239), and the Cuiying Foundation.

References

[1] R. Waser, M. Aono, Nature Mater. 6 (2007) 833.
[2] Y.C. Yang, F. Pan, Q. Liu, M. Liu, F. Zeng, Nano Lett. 9 (4) (2009) 1636.
[3] Y. Li, S. Long, M. Zhang, Q. Liu, L. Shao, S. Zhang, Y. Wang, Q. Zuo, S. Liu, M. Liu, IEEE Electron Device Lett. 31 (2) (2010) 117.
[4] C. Li, D. Belkin, Y. Li, P. Yan, M. Hu, N. Ge, H. Jiang, E. Montgomery, P. Lin, Z. Wang, W. Song, J.P. Strachan, M. Barnell, Q. Wu, R.S. Williams, J.J. Yang, Q. Xia, Nature Commun. 9 (1) (2018) 2385.
[5] X. Zhao, J. Ma, X. Xiao, Q. Liu, L. Shao, D. Chen, S. Liu, J. Niu, X. Zhang, Y. Wang, R. Cao, W. Wang, Z. Di, H. Lv, S. Long, M. Liu, Adv. Mater. 30 (14) (2018) 1705193.
[6] H. Shima, F. Takano, H. Muramatsu, H. Akinaga, I.H. Inoue, H. Takagi, Appl. Phys. Lett. 92 (4) (2008) 043510.

[7] C. Rohde, B.J. Choi, D.S. Jeong, S. Choi, J.-S. Zhao, C.S. Hwang, Appl. Phys. Lett. 86 (26) (2005) 262907.
[8] W. Wang, S. Fujita, S.S. Wong, IEEE Electron Device Lett. 30 (7) (2009) 763.
[9] J.J. Yang, F. Miao, M.D. Pickett, D.A.A. Ohlberg, D.R. Stewart, C.N. Lau, R.S. Williams, Nanotechnology 20 (21) (2009) 215201.
[10] J.J. Yang, M.D. Pickett, X. Li, D.A.A. Ohlberg, D.R. Stewart, R.S. Williams, Nature Nanotechnol. 3 (7) (2008) 429.
[11] Y. Lu, B. Gao, Y. Fu, B. Chen, L. Liu, X. Liu, J. Kang, IEEE Electron Device Lett. 33 (3) (2012) 306.
[12] B. Gao, S. Yu, N. Xu, L.F. Liu, B. Sun, X.Y. Liu, R.Q. Han, J.F. Kang, B. Yu, Y.Y. Wang, 2008 IEEE International Electron Devices Meeting, 2008, p. 1.
[13] G.H. Baek, A.R. Lee, T.Y. Kim, H.S. Im, J.P. Hong, Appl. Phys. Lett. 109 (14) (2016) 143502.
[14] C.C. Hsieh, A. Roy, A. Rai, Y.F. Chang, S.K. Banerjee, Appl. Phys. Lett. 106 (17) (2015) 173108.
[15] A. Padovani, L. Larcher, O. Pirrotta, L. Vandelli, G. Bersuker, IEEE Trans. Electron Devices 62 (6) (2015) 1998.
[16] K. Jalili, S. Aghabeygi, B. Mirza, J. Appl. Chem. Res. 10 (4) (2016) 123.
[17] E.N. Plotnikov, V.L. Stolyarova, Phys. Chem. Glasses 46 (2) (2005) 187.
[18] W. Wu, X. Duan, J.S. Yuan, IEEE Trans. Device Mater. Reliab. 3 (2) (2003) 26.
[19] S. Srivastava, P. Dey, S. Asapu, T. Maiti, Nanotechnology 29 (50) (2018) 505702.
[20] D. Mardare, C. Baban, R. Gavrila, M. Modreanu, G. Rusu, Surf. Sci. 507–510 (2002) 468.
[21] P. Bousoulas, I. Giannopoulos, P. Asenov, I. Karageorgiou, D. Tsoukalas, J. Appl. Phys. 121 (9) (2017) 094501.
[22] S. Yu, H.P. Wong, IEEE Electron Device Lett. 31 (12) (2010) 1455.